Simultaneous measurement of neutron-induced fission and capture cross sections for ^{241}Am at neutron energies below fission threshold

K. Hirose[a], K. Nishio[a], H. Makii[a], I. Nishinaka[a], S. Ota[a], T. Nagayama[a,b], N. Tamura[a,c], S. Goto[c], A.N. Andreyev[a,d], M.J. Vermeulen[d,1], S. Gilespie[d], C. Barton[d], A. Kimura[e], H. Harada[e], S. Meigo[f], S. Chiba[g], T. Ohtsuki[h]

[a] *Advanced Science Research Center, Japan Atomic Energy Agency (JAEA), Tokai, Ibaraki 319-1195, Japan*
[b] *Graduate School of Science and Engineering, Ibaraki University, Mito 310-0056, Japan*
[c] *Graduate School of Science and Technology, Niigata University, Niigata 950-2181, Japan*
[d] *Department of Physics, University of York, Heslington, York, YO10 5DD, United Kingdom*
[e] *Nuclear Science and Engineering Center, JAEA, Tokai, Ibaraki 319-1195, Japan*
[f] *J-PARC Center, JAEA, Tokai, Ibaraki 319-1195, Japan*
[g] *Research Laboratory for Nuclear Reactors, Tokyo Institute of Technology, Tokyo 152-8550, Japan*
[h] *Research Reactor Institute, Kyoto University, Kumatori-cho, Sennangun, Osaka 590-0494, Japan*

Abstract

Fission and capture reactions were simultaneously measured in the neutron-induced reactions of ^{241}Am at the spallation neutron facility of the Japan Proton Accelerator Research Complex (J-PARC). Data for the neutron energy range of $E_n = 0.1$–$20\,\mathrm{eV}$ were taken with the TOF method. The fission events were observed by detecting prompt neutrons accompanied by fission using liquid organic scintillators. The capture reaction was measured by detecting γ rays emitted in the deexcitation of the compound nuclei using the same detectors, where the prompt fission neutrons and capture γ rays were separated by a pulse shape analysis. The cross sections were obtained by normalizing the relative yields at the first resonance to evaluations or other experimental data. The ratio of the fission to capture cross sections at each resonance is compared with those from an evaluated nuclear data library and other experimental data. Some differ-

Email address: hirose.kentaro@jaea.go.jp (K. Hirose)

ences were found between the present values and the library/literature values at several resonances.

Keywords: ^{241}Am, neutron-induced fission, neutron capture, time-of-flight method, pulse shape analysis

1. Introduction

Management of minor actinides (MAs) such as neptunium, americium and curium isotopes generated in nuclear power plants is one of the most important issues in the use of nuclear energy. Because of the long half-lives of these radioactive nuclides, an extremely long time is necessary to confine the high-level nuclear wastes. Transmutation of MAs in a critical system such as Gen-IV type reactors or an accelerator-driven subcritical system is actively discussed to reduce the amount of these nuclear wastes and to shorten the confinement period. Design of these transmutation systems necessitates nuclear data for such minor actinides, *e.g.* fission and capture cross sections with higher accuracy.

Measurements of fission cross section (σ_f) are mostly based on the detection of fission fragments. Various types of gaseous detectors such as Frisch-grid ionization chambers [1, 2], fast ionization chambers [3, 4], and parallel plate avalanche detectors [5, 6] were used. In an experiment at ORELA [7] fission fragments could not be directly detected, therefore the prompt neutrons accompanied by fission were measured. Neutron capture cross sections (σ_γ) have been measured by detecting capture γ rays, for example, using scintillation crystals such as NaI and BaF_2 [8–10]. Liquid C_6D_6 scintillation detectors [11, 12] or Ge detectors [13, 14] were also used.

Measurements of fission or capture cross sections have usually been carried out independently with different detector setups. In the present work, we simultaneously measured both fission and capture reactions in the same setup using liquid organic scintillators. The cross sections were measured at the neutron energies far below the fission threshold, where fission cross sections are about two orders of magnitude smaller than the capture cross sections. Fission events were

identified by detecting prompt fission neutrons. Detected γ rays are assumed to originate from the capture process because the number of prompt fission γ rays is far smaller due to low fission cross sections. A pulse shape analysis of the scintillator signals was applied to separate prompt neutron and γ-ray events.

Since the experimental condition to measure σ_f and σ_γ are completely the same in the present method, some of error sources and corrections given in the data analysis are principally the same. Some of the examples are self-shielding of neutrons by the target, a correction for dead-time associated with detector response and data acquisition procedure. Thus, the ratio of both cross sections, σ_f/σ_γ, obtained in this experiment principally does not contain systematic errors as a result of cancellation of common errors. Experimental data obtained in this manner would improve analysis of resonance parameters of σ_f and σ_γ to discuss intermediate structure in the sub-barrier fission [15] originating from coupling between class I and class II states in the double-humped fission barrier [16].

2. Experimental method and setup

The experiment was performed at the Materials and Life science Facility (MLF) of J-PARC. A high-intensity pulsed neutron beam was produced by spallation reactions in a mercury target irradiated with 3-GeV protons (25-Hz repetition, 200-kW power). Neutrons were slowed down in a hydrogen moderator and transported to the fourth beam line in MLF (BL04 course), which is designed for neutron time-of-flight (TOF) measurements. The beam line consists of collimators, a neutron chopper and resonance filters. The neutron chopper was used to reduce the flux of slow neutrons which were produced in the previous proton pulse and entered in the TOF interval defined by the latest pulse (wrap-around neutrons). The flight distance in this experiment was 21.5 m. More details about the beam line are given in Ref. [17].

The experimental setup is illustrated in Fig. 1. The americium target contains 7.5 mg of ^{241}Am (952 MBq) in a chemical form of dioxide. The isotopic pu-

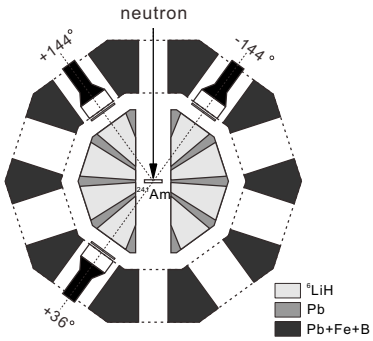

Figure 1: Schematic layout of the experimental setup. Three NE213-type scintillators are placed in holes of the neutron shield.

rity is 99.99%. The ratio of the total radio-activity of the impurities of $^{239-241}$Pu to that of ^{241}Am is less than 1×10^{-2}%. The mass fraction of non-radioactive impurities is less than 0.2%. The mixture of the americium dioxide and aluminum metal powder was pressed into a pellet shape of 10-mm diameter and 1-mm thickness. The pellet was enclosed in an aluminum container.

Three NE213-type scintillators, 101.6 mm in diameter and 50.8 mm in length, were placed at angles of $+36°$, $+144°$ and $-144°$ with respect to the beam direction. The distance from the center of the target to the detector surface was 150 mm. Scattered neutrons having energies below 20 eV (the energy range of this measurement is $E_n = 0.1 - 20$ eV) do not directly disturb the detection of the prompt fission neutrons with an average energy of 1 MeV. The scattered neutrons however cause additional γ-ray background by capture reactions. To reduce the background, two kinds of shields were used. One is made of lithium hydride powder enclosed in a cone-shaped aluminum container and placed between the target and the detectors (^{6}LiH in Fig. 1) to stop scattered neutrons from the target. The other is layers of lead, iron and borax resin to shield the neutrons and γ rays entering from other directions, where 478-keV γ rays from the most inner layer of the borax resin are shielded by the outer layers of lead and iron. In addition, lead plates of 1.6-mm thickness were placed just in front of the detectors to suppress low energy γ and X rays from the radio-activity of

^{241}Am.

The anode signals from the photomultipliers were analyzed using the MPD-4 module (Mesytec GmbH &Co. KG, Germany) which gives an amplified signal as well as a pulse-shape signal, *i.e.*, a time difference between the leading and the trailing edges of the input signal. The amplified and the pulse-shape signals were recorded using the A3400-PDC (peak-to-digital converter) module (NIKI GLASS Co., Ltd., Japan) and recorded with the elapsed time from the proton pulse for the TOF analysis of fission and capture events.

In the neutron capture process, the average γ-ray multiplicity is typically 3–4 [18, 19]. In the thermal-neutron fission of ^{239}Pu, for example, 6.9 γ rays per fission are emitted on average with an average energy of 1.0 MeV [20]. The average total γ-ray energy per fission, $\sim$ 7 MeV, was also obtained in more recent measurement for the spontaneous fission of ^{252}Cf and the thermal-neutron fission of ^{235}U, ^{241}Pu [21]. Considering that the fission cross section for ^{241}Am is two orders of magnitude smaller than the capture cross section [22] in the neutron energy region of this measurement ($E_n < 20$ eV), γ rays detected in the scintillators are assumed to originate from the neutron capture process.

3. Experimental results and discussions

Figure 2(a) and 2(b) show two dimensional plots of the pulse height versus the pulse shape, where neutron and γ-ray events are clearly separated. They are obtained using the ^{241}Am target and an empty aluminum disk, respectively. Figure 2(c) shows the projections of the two dimensional plots along with the curvature of the γ-ray events indicated by the dashed curve in Fig. 2(a) and 2(b). The neutron yield is clearly seen in the case of the ^{241}Am target. Events in the pulse shape of 700–1500 ch were selected as γ-ray events whereas those in 1750–3000 ch as neutron events. These selections correspond to the region marked by γ and n in the figure. The upper limit of the pulse-height selection was set to 6000 ch which is equivalent to the Compton edge of 7.72-MeV γ rays from the ^{27}Al(n, γ) reaction. This selection does not influence the ^{241}Am(n, γ)

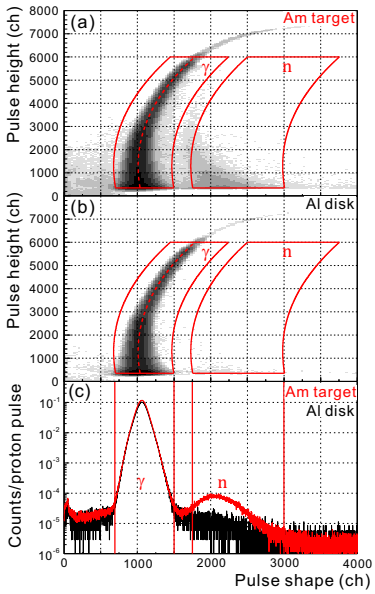

Figure 2: (a) Correlation between the pulse shape and the pulse height observed in the measurement of ^{241}Am. (b) same as (a) but obtained in the measurement of the aluminum disk. (c) Projection of (a) and (b) on the horizontal axis along with the γ-ray locus.

events, because the neutron separation energy of ^{242}Am is 5.54 MeV and the incident neutron energy used in this analysis is lower than 20 eV. The lower limit of the pulse height is set to 220 keVee (350 ch), see Fig 2(a) and 2(b).

The TOF spectra for the neutron and the γ-ray events are shown in Fig. 3. The spectra were obtained by two scintillators placed at the backward direction of $\pm 144°$. The forward scintillator was not used in this analysis, because clear separation between neutrons and γ rays was not obtained due to the γ flash.

Assuming the non-extended dead-time model [23], the true counting rate at time t is given by $R_0(t) = R(t)/\{1 - \int_{t-\tau}^{t} R(t')dt'\}$, where $R(t)$ is the observed counting rate at t. Using the dead-time $\tau = 400$ ns which is required for the data acquisition module to process one signal, the dead-time correction was estimated to be 0.8% at the first resonance ($E_r = 0.305$ eV), 1.0% at the second resonance (0.572 eV) and 1.9% at the third resonance (1.27 eV). The applied dead-time correction is neutron-energy dependent and the same for the neutron

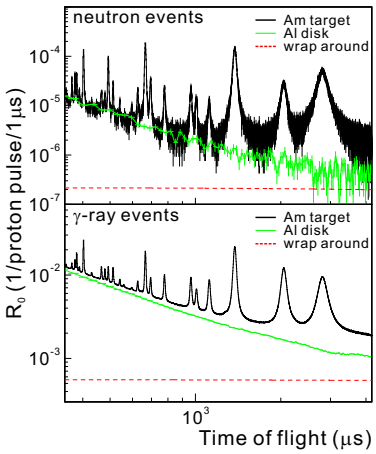

Figure 3: TOF spectra for neutron and γ-ray events. Thin and dashed lines show the background from the Al disk and the wrap-around background, respectively.

and γ-ray events.

Background due to the wrap-around neutrons was estimated in the same manner as described in Ref. [24]. The background spectrum due to the wrap-around neutrons is expressed by a combination of an exponential function and a constant which includes the background from the decay of ^{241}Am. The dashed line in Fig. 3 is the deduced wrap-around background. It was estimated to be 0.4, 1.5 and 0.5% for the neutron events, and 2.7, 4.8 and 6.2% for the γ-ray events at the first three resonances, respectively. The background was subtracted depending on the incident neutron energy.

Background from the aluminum material contained in the ^{241}Am target was estimated by the measurement of the aluminum disk. The data were analyzed in the same way as for the ^{241}Am target described above. The background from the aluminum disk is shown by the thin line in Fig. 3 and estimated to be 1.0, 3.3 and 1.1% for the neutron events, and 13, 14 and 11% for the γ-ray events at the first three resonances.

After subtracting the backgrounds, the self-shielding effect was corrected. The correction factor is defined as a ratio of the incident neutron flux to the

average neutron flux taken over the target thickness, *i.e.*,

$$\eta(E_n) = \frac{\sigma(E_n)\rho}{1 - e^{-\sigma(E_n)\rho}}, \tag{1}$$

where σ is the absorption cross section (fission + capture) and ρ is the number density of nuclei per unit area. In addition, an effect of the scattered neutrons was also considered for the γ-ray events. The scattered neutrons in the target pass through longer distance in the target and some of them will be captured. This effect was calculated using a Monte Carlo simulation code PHITS [25]. For the neutron events, only the self-shielding effect was considered because the fission cross section is much lower than the capture cross section. By referring to the cross sections from JENDL-4.0, η was estimated to be 1.071, 1.061 and 1.078 at the first three resonances, respectively.

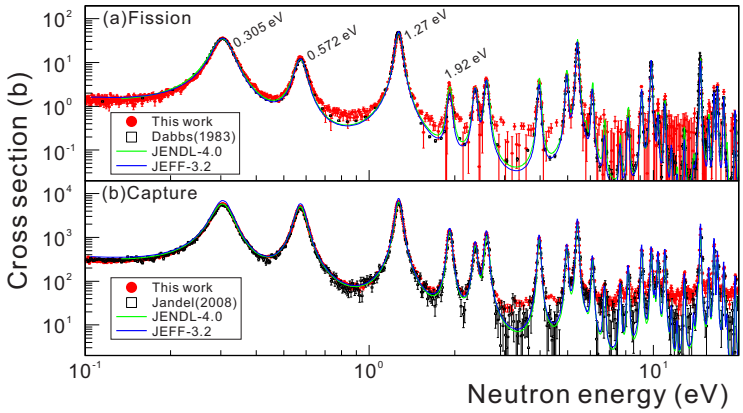

Figure 4: (a) The cross section of ^{241}Am(n, f) obtained in the present work (closed circles) is compared with the data by Ref. [26] (open squares) and the JENDL-4.0 and the JEFF-3.2 evaluations (solid curves). (b) The cross section of ^{241}Am(n, γ) (closed circles) is compared with the data by Ref. [18] (open squares) and the JENDL-4.0 and the JEFF-3.2 evaluations (solid curves).

After finishing the procedure described above, the neutron-energy dependent spectra for fission and capture events are divided by the neutron spectrum [17] to obtain the relative values of their cross sections. To give absolute values of the cross sections, the spectra are normalized such that the first resonance

integrated over 0.208–0.403 eV for fission and capture give the same values as the JENDL-4.0 library data.

The obtained σ_f is shown by the closed circles in Fig. 4(a). The open squares were the experimental data by Dabbs [26]. The evaluations of JENDL-4.0 [22] and JEFF-3.2 [27] are also shown for comparison. It was reported that the average neutron multiplicity in fission $\bar{\nu}$ slightly changes with the incident neutron energy for ^{235}U(n, f) and ^{239}Pu(n, f) [28, 29]. This effect was not taken into account in the present analysis because it has not been studied for ^{241}Am(n, f) up to now. The ratios for the fission cross sections of the other data to our data are summarized in Table 1 and Fig. 5(a) where the cross sections are integrated around the resonance energies E_r. The range of the integration is from E_1 to E_2, which was determined from the full width at 20% maximum of each resonance by referring to the total width compiled in the JENDL-4.0 library. The third to fifth columns are the cross section ratios to this work for JENDL-4.0 [22], JEFF-3.2 [27] and for the experimental data by Dabbs [26], respectively. Each ratio at the first resonance (E_r=0.305 eV) is normalized to unity to compare independently on what we use for the cross section normalization. The values in the parentheses in the top row are the normalization factors when our data is normalized to JENDL-4.0. Only the statistical errors for our data and the errors given in Ref. [26] are considered. The valuse in JEFF-3.2 are similar to those of Ref. [26]. All of JENDL-4.0, JEFF-3.2 and Ref. [26] show smaller values than the present data at E_r=0.572 by $\sim$ 10% and 2.60 eV by $\sim$ 15%. Althogh JENDL-4.0 agrees with the present work better than JEFF-3.2 at E_r=1.92, 2.36 and 14.7 eV, The JEFF-3.2 evaluation shows slightly better agreement with the present data in total (see Fig. 5(a)).

The neutron capture cross section obtained in the present work is shown by the closed circles in Fig. 4(b). The experimental data by Jandel [18] and the evaluations of JENDL-4.0 and JEFF-3.2 are also shown. In measurements where not all of the γ rays from a capture event are detected as in the present experiment, the pulse-height weighting (PHW) technique [30] is generally applied in the analysis in order to consider that the number of emitted γ rays depends on

Table 1: Ratios of $\left[\int_{E_1}^{E_2} \sigma_f \, dE\right]_{\text{others}} \Big/ \left[\int_{E_1}^{E_2} \sigma_f \, dE\right]_{\text{This work}}$ are summarized. The first column is the resonance energy and the second are the lower and upper energies of the resonance integration. The ratios are normalized at the first resonance E_r=0.305 eV.

E_r (eV)	E_1/E_2 (eV)	$\frac{\text{JENDL}}{\text{This work}}$ (1.000*)	$\frac{\text{JEFF}}{\text{This work}}$ (0.976*)	$\frac{\text{Dabbs}}{\text{This work}}$ (1.007*)
0.305	0.208/0.403	1.00±0.01	1.00±0.01	1.00±0.01
0.572	0.478/0.667	0.90±0.01	0.91±0.01	0.90±0.01
1.27	1.17/1.37	0.98±0.01	1.02±0.01	1.00±0.01
1.92	1.83/2.01	1.05±0.08	0.73±0.06	0.81±0.06
2.36	2.25/2.47	0.99±0.08	0.91±0.07	0.95±0.08
2.60	2.49/2.70	0.87±0.05	0.86±0.05	0.82±0.05
3.97	3.87/4.07	1.14±0.09	0.82±0.06	0.82±0.06
4.97	4.87/5.06	1.24±0.08	0.99±0.07	0.99±0.07
5.42	5.32/5.51	1.18±0.02	1.02±0.02	0.98±0.03
9.85	9.75/9.95	1.06±0.06	1.05±0.06	0.99±0.06
14.7	14.6/14.8	0.96±0.05	0.78±0.04	0.89±0.38

* These values are the normalization factors when our data are fixed to JENDL-4.0 evaluation at the first resonance.

the resonances. In the present analysis, we found that σ_γ obtained using the PHW technique with a simple weighting function [24] agrees with that obtained without PHW within the statistical uncertainty. Therefore the cross section obtained without applying the PHW technique is shown in Fig. 4(b). Table 2 and Fig. 5(b) shows the capture cross section ratios to our data for the evaluations of JENDL and JEFF, and the recent experimental data by Jandel [18], Lampoudis [31] and by Fraval [12]. The statistical errors of this work and the uncertainty given in Jandel [18] are considered here. Discrepancies between our data and the experimental data by Jandel or Fraval increases in the region $E_n > 2$ eV. The JENDL-4.0 evaluation is systematically smaller by 15% above 2 eV. In Fig. 4(b) one can see that the present data have larger values at the energies between resonances in the region $E_n > 3$ eV. The main reason would be an insufficient subtraction of background γ rays produced outside the target,

Table 2: Ratios of $\left[\int_{E_1}^{E_2}\sigma_\gamma\,dE\right]_{\text{others}}\Big/\left[\int_{E_1}^{E_2}\sigma_\gamma\,dE\right]_{\text{This work}}$ are summarized. The first column is the resonance energy and the second are the lower and upper energies of the resonance integration.

E_r (eV)	E_1/E_2 (eV)	$\frac{\text{JENDL}}{\text{This work}}$ (1.000*)	$\frac{\text{JEFF}}{\text{This work}}$ (1.129*)	$\frac{\text{Jandel}}{\text{This work}}$ (0.9411*)	$\frac{\text{Lampoudis}}{\text{This work}}$ (1.136*)	$\frac{\text{Fraval}}{\text{This work}}$ (0.8384*)
0.305	0.208/0.403	1.000±0.001	1.000±0.001	1.000±0.009	1.000±0.001	1.000±0.001
0.572	0.478/0.667	0.989±0.002	0.979±0.002	0.974±0.013	0.975±0.002	0.985±0.002
1.27	1.17/1.37	0.948±0.002	0.984±0.002	0.969±0.017	0.966±0.002	0.952±0.002
1.92	1.83/2.01	0.889±0.006	0.944±0.006	0.945±0.044	0.942±0.006	0.993±0.007
2.36	2.25/2.47	0.872±0.012	0.914±0.013	0.917±0.062	0.970±0.013	1.057±0.015
2.60	2.49/2.70	0.830±0.007	0.932±0.008	0.870±0.049	0.941±0.008	0.903±0.008
3.97	3.87/4.07	0.851±0.010	0.937±0.011	0.866±0.065	0.905±0.011	0.910±0.011
4.97	4.87/5.06	0.846±0.015	0.894±0.016	0.830±0.085	0.879±0.016	0.824±0.015
5.42	5.32/5.51	0.884±0.006	0.976±0.006	0.818±0.045	0.949±0.006	0.689±0.004
9.85	9.75/9.95	0.816±0.020	0.875±0.022	0.684±0.088	0.903±0.023	0.768±0.019
14.7	14.6/14.8	0.852±0.015	0.978±0.017	0.590±0.051	1.019±0.018	0.154±0.003

* These values are the normalization factors when our data are fixed to JENDL-4.0 evaluation at the first resonance.

such as capture γ rays from a beam duct. The background level in this energy region is roughly estimated to be 30–50 barn which results in enhancement of about 10% in the cross section integral for σ_γ. Then the JEFF-3.2 evaluation and the data by Lampoudis seem to show the best agreement with our data among them.

In the present work, the common uncertainties due to the dead-time correction, the self-shielding correction and the neutron spectrum are canceled in the cross-section ratio between fission and capture. Hence the simultaneous measurement demonstrated in this study will be useful to measure smaller fission cross sections such as ^{237}Np and ^{243}Am where a thick target is needed and then the corrections mentioned above should be larger.

The ratio of the cross sections is defined as $R_s \equiv \left[\int_{E_1}^{E_2}\sigma_f\,dE_n\right]/\left[\int_{E_1}^{E_2}\sigma_\gamma\,dE_n\right]$,

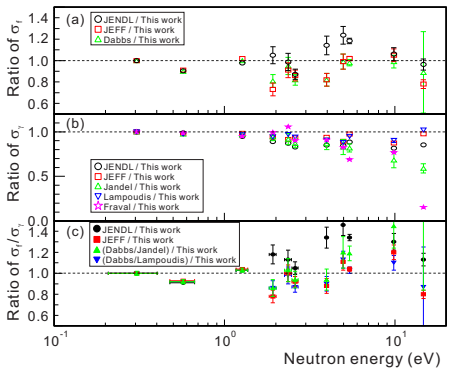

Figure 5: (a) The fission cross-section ratios between the other data and the present work summarized in Table. 1. (b) The caputure cross-section ratios between the other data and the present work summarized in Table. 2. (c) The ratio of R_s values, see text and Table 3. The horizontal bars denote the range of the integration.

where $E_{1,2}$ are the same as described before. In order to compare the cross-section ratio obtained in this study $R_s^{\text{This work}}$, the ratios of the cross-section ratio are plotted in Fig. 5(c). All symbols are the ratios of R_s obtained from the evaluations and the experimental data to that of this work $R_s^{\text{This work}}$. Closed circles and squares show $R_s^{\text{JENDL}}/R_s^{\text{This work}}$ and $R_s^{\text{JEFF}}/R_s^{\text{This work}}$, respectively. Closed triangles and reverse triangles show the ratio between the other experimental data and our data. The data by Dabbs [26] were used for the fission cross sections and the data by Jandel [18] and by Lampoudis [31] were used for the capture cross sections. The horizontal bars in Fig. 5(c) denote the range of this integration. The values are also summarized in Table 3. Since the absolute values of our cross sections are arbitrary, the ratios are normalized to unity at the first resonance. The values in the parentheses at the top row in Table 3 are the normalization factors when our data are fix to the JENDL-4.0 evaluation. Smaller $R_s/R_s^{\text{This work}}$ values are found at the second resonance (E_r=0.572 eV) for all compared libraries and the experiments. This is mainly attributed to their σ_f which are smaller by 9–10%, while their σ_γ are smaller by only 1–3%. For the fourth resonance (E_r=1.92 MeV), $R_s/R_s^{\text{This work}}$ values except for JENDL-4.0 are smaller by 14–22%. This is because of their smaller σ_γ and even

Table 3: Ratios of the cross-section ratio $\left[\int_{E_1}^{E_2}\sigma_f\,dE\right]\Big/\left[\int_{E_1}^{E_2}\sigma_\gamma\,dE\right]$ ($\equiv R_s$) are summarized. The first column is the resonance energy and the second are the lower and upper energies of the resonance integration, see also Fig. 5(c). The third to sixth columns are the ratios of the R_s values obtained in this work to that of JENDL-4.0, JEFF-3.2 and the other experimental data in [18, 26, 31], respectively.

E_r (eV)	E_1/E_2 (eV)	$\frac{R_s^{\rm JENDL}}{R_s^{\rm This\ work}}$ (1.000*)	$\frac{R_s^{\rm JEFF}}{R_s^{\rm This\ work}}$ (0.864*)	$\frac{R_s^{\rm Ref.\ [18,\ 26]}}{R_s^{\rm This\ work}}$ (1.070*)	$\frac{R_s^{\rm Ref.\ [26,\ 31]}}{R_s^{\rm This\ work}}$ (0.886*)
0.305	0.208/0.403	1.00±0.01	1.00±0.01	1.00±0.02	1.00±0.01
0.572	0.478/0.667	0.91±0.01	0.93±0.01	0.92±0.02	0.92±0.01
1.27	1.17/1.37	1.03±0.01	1.04±0.01	1.03±0.02	1.03±0.01
1.92	1.83/2.01	1.18±0.09	0.78±0.06	0.86±0.08	0.86±0.07
2.36	2.25/2.47	1.13±0.09	1.00±0.08	1.03±0.11	0.98±0.08
2.60	2.49/2.70	1.05±0.06	0.92±0.05	0.94±0.08	0.87±0.05
3.97	3.87/4.07	1.34±0.10	0.88±0.07	0.94±0.10	0.90±0.07
4.97	4.87/5.06	1.46±0.10	1.11±0.08	1.20±0.15	1.13±0.08
5.42	5.32/5.51	1.34±0.03	1.04±0.02	1.19±0.07	1.03±0.03
9.85	9.75/9.95	1.30±0.08	1.20±0.07	1.45±0.21	1.10±0.07
14.7	14.6/14.8	1.13±0.06	0.80±0.04	1.50±0.66	0.87±0.38

* These values are the normalization factors when our data are fixed to JENDL-4.0 evaluation at the first resonance.

smaller σ_f, see Tables 1, 2. The JEFF-3.2 evaluation can reproduce the present data better than JENDL-4.0 in total.

In the analysis we assumed that the average neutron multiplicity in fission, $\bar{\nu}$, does not change through the measured incident-neutron energy range. The assumption is based on the measurement of $\bar{\nu}$ for ^{235}U(n,f) [29] where the difference of $\bar{\nu}$ for each resonance from the average was found to be within ±0.8%. A maximum deviation (7.3 ± 1.0)% for $\bar{\nu}$ from the average over the energy range E_n=7–400 eV was found in ^{239}Pu(n,f) [28]. The differences in R_s for some resonances found in between the present data and literature/library data are larger than the change of $\bar{\nu}$ observed so far.

4. Summary

We have measured the ^{241}Am(n, f) and the (n, γ) reactions in the same experimental setup. Owing to the high intensity neutron beam at J-PARC, fission events were successfully observed by detecting prompt neutrons using liquid scintillators. In the simultaneous measurement, the corrections for the dead time, self-shielding and the neutron spectrum have common values for both fission and capture cross sections, which would result in significant reduction of the error in the cross section ratio between fission and capture, R_s. For example the self-shielding correction gives a relatively large correction factor (6–8%) in this analysis. Ambiguities from these corrections are all canceled in the cross-section ratio. From the measurement of n+^{241}Am, it is found that the R_s value from the literature data at the second resonance (E_r=0.572 eV) is about 8% smaller than that obtained in the present work. On the other hand, the values from JENDL-4.0 at the higher energy resonances (E_r=4.97, 5.42 and 9.85 eV) are 30–46% larger than the present data. Although this is partly due to apparently larger, roughly 10%, σ_γ obtained in this work mentioned before, the discrepancy cannot be explained only by the background of this measurement. The deviations are larger than the fluctuation of average prompt neutrons $\bar{\nu}$ investigated in neutron-induced fission of ^{235}U and ^{239}Pu. We will start a more detailed fission study by detecting the fission fragments in coincidence with the prompt neutrons/γ rays after the permission to use unsealed radioactive materials as a target is given.

Acknowledgements

The authors would like to thank the accelerator and technical staff at J-PARC for operation of the accelerator and the neutron production target and for the other experimental supports.

References

[1] P. Salvador-Castiñeira, Phys. Rev. C **92**, 014620 (2015).

[2] F. Tovesson *et al.*, Phys. Rev. Lett. **88**, 062502 (2002)

[3] M. Calviani *et al.*, Nucl. Instru. Meth. A, **594**, 220 (2008).

[4] D. Karadimos *et al.*, Phys. Rev. C **89**, 044606 (2014).

[5] C. Paradela *et al.*, Phys. Rev. C **82**, 034601 (2010).

[6] F. Tovesson and T.S. Hill, Phys. Rev. C **75**, 034610 (2007).

[7] M.S. Moore *et al.*, Phys. Rev. C **18**, 1328 (1978).

[8] S. Mosby *et al.*, Phys. Rev. C, **89**, 034610 (2014).

[9] E. Mendoza *et al.*, Phys. Rev. C, **90**, 034608 (2014).

[10] C. Guerrero *et al.*, Nucl. Instrum. Meth. A **608**, 424 (2009).

[11] C. Lederer *et al.*, Phys. Rev. Lett. **110**, 022501 (2013).

[12] K. Fraval *et al.*, Phys. Rev. C, **89**, 044609 (2014).

[13] A. Kimura *et al.*, J. Nucl. Sci. Technol. **49**, 708 (2012).

[14] H. Harada *et al.*, Nucl. Data Sheet **119**, 61 (2014).

[15] M.S. Moore and G.A. Keyworth, Phys. Rev. C **3**, 1656 (1971)

[16] S. Bjørnholm and J.E. Lynn, Rev. Mod. Phys., **52**, 725 (1980).

[17] K. Kino *et al.*, Nucl. Instr. and Meth. A **626-627**, 58 (2011)

[18] M. Jandel *et al.*, Phys. Rev. C **78**, 034609 (2008)

[19] A. Chyzh *et al.*, Phys. Rev. C **88**, 044607 (2013)

[20] F. Pleasonton *et al.*,, Nucl. Phys. A **213**, 413 (1973).

[21] S. Oberstedt *et al.*, Eur. Phys. J. A **51**, 178 (2015)

[22] K. Shibata *et al.*, J. Nucl. Sci. Technol. **48**, 1 (2011)

[23] J.W. Müller, Nucl. Instr. and Meth. **112**, 47 (1973)

[24] K. Hirose *et al.*, J. Nucl. Sci. Technol. **50** 188–200 (2013)

[25] K. Niita *et al.*, JAEA-Data/Code 2010-022 (2010).

[26] J.W. T. Dabbs *et al.*, Nucl. Sci. Eng. **83**, 22 (1983)

[27] https://www.oecd-nea.org/dbdata/jeff/

[28] J. Fréhaut and D. Shakelton, *Proceedings of 3rd Symposium of Physics and Chemistry of Fission*, IAEA Vienna, 201 (1974)

[29] R.E. Howe, T.W. Phillips and C.D. Bowman, Phys. Rev. C **13**, 195 (1976)

[30] R. L. Macklin and J. H. Gibbons, Phys. Rev. **159**, 1007 (1967)

[31] C. Lampoudis *et al.*, Eur. Phys. J. Plus **128**, 86 (2013)

[32] Table of Radioactive Isotopes, http::/ie.lbl.gov/toi/radSearch.asp, Lawrence Berkeley National Laboratory